Journal of Applied Polymer Science

Synthesis of a montmorillonite-supported titania nanocomposite with grafted cellulose as a template and its application in photocatalytic degradation

Xiaolin Man,[1] Ronglan Wu,[1] Henghua Lv,[1] Wei Wang[1,2]

[1]Key Laboratory of Oil and Gas Fine Chemicals, Ministry of Education and Xinjiang Uyghur Autonomous Region, College of Chemistry and Chemical Engineering, Xinjiang University, Urumqi Xinjiang 830046, China

[2]Centre for Pharmacy and Department of Chemistry, University of Bergen, N-5007 Bergen, Norway

Correspondence to: R. Wu (E-mail: wuronglan@163.com) and W. Wang (E-mail: wei.wang@kj.uib.no)

ABSTRACT: We report a study on the synthesis of anatase titania (TiO_2) particles with the sol–gel method at room temperature. We immobilized the particles on a grafted-cellulose intercalated montmorillonite (MMT). This nanocomposite, cellulose-*g*-poly(4-vinyl pyridine)/MMT/TiO_2, could be applied in the photocatalytic degradation of organic pollutants efficiently because of the addition of a sorbent, the grafted cellulose. The synthesized nanocomposite was characterized with Fourier transform infrared spectroscopy, X-ray diffraction, scanning electron microscopy, and transmission electron microscopy. Methyl orange was used as a model molecule to study photocatalytic degradation. The nanocomposite exhibited a better photocatalytic activity than in the absence of the grafted cellulose. The kinetics of the photocatalytic degradation could be described by pseudo-first-order rate law. © 2015 Wiley Periodicals, Inc. J. Appl. Polym. Sci. **2015**, *132*, 42627.

KEYWORDS: adsorption; cellulose and other wood products; colloids

Received 24 March 2015; accepted 15 June 2015
DOI: 10.1002/app.42627

INTRODUCTION

Titania (TiO_2), a semiconductor, is commonly used as a photocatalyst in light-induced photochemical reactions because of its unique electronic structure.[1] The electronic structure of TiO_2 is characterized by a filled valence band and an empty conduction band. In a redox reaction, the redox potential for the formation of reactive oxygenated species lies within the band gap of the semiconductor and can be catalyzed by TiO_2.[2] This initiates applications of TiO_2 in two main respects: water electrolysis and waste treatments. As a catalyst, a high surface area and stability are required. This calls for research in fabrication of TiO_2 particles with different morphologies and the immobilization of TiO_2 powders. Hitherto, much attention has been paid to the synthesis of TiO_2 with morphology-controlled methods, such as in nanowires,[3] nanorods,[4] nanotubes,[5] and flowerlike microspheres.[6] As for the templates used in synthesis of TiO_2 particles, these include natural cellulose,[7,8] natural rubber,[9] polymer fibers,[10] macroporous silica,[11] and so forth.[7]

For the purpose of handling photocatalysts, TiO_2 powders are often immobilized on a matrix.[2] Immobilized TiO_2 powders exhibit a better thermal stability and mechanical strength; this results in enhanced photocatalysis.[12,13] For example, through the addition of a small amount of clay, the dispersity and the stability of TiO_2 improves, and the aggregation of TiO_2 nanoparticles is also effectively prevented.[14] These fundamental concerns are all considered in the applications of TiO_2 nanocomposites in the photocatalytic decomposition of pollutants. However, the purification of three-dimensional spaces by photocatalysis encounters many impediments because of the nature of the photocatalysis.[1] The photocatalysis occurs on the surface of the catalyst. Reactants are must be in the vicinity of the particle surface to be captured by the photocatalyst. The application of a photocatalyst in wastewater treatment by the random collision of the particles and pollutants renders very low efficiency.[2]

Natural cellulose is a green template for the synthesis of TiO_2 nanoparticles. Neat cellulose often has a poor adsorption capacity, whereas an important step of photodegradation is that pollutant molecules must be gathered over the surface of TiO_2. Thus studies of grafted cellulose to improve the adsorption capacity have attracted much attention.[15] In this study, anatase TiO_2 particles were prepared at a low temperature with grafted cellulose as a template. The particles were then immobilized on montmorillonite (MMT). In this nanocomposite, the grafted cellulose acted as a sorbent and formed complexes with

organic dyes. Subsequently, the organic pollutes were gathered over on the surface of TiO_2 and degraded by the photocatalytic reaction.

EXPERIMENTAL

Materials

Cellulose (bamboo pulp) was purchased from Beiyan Yasong Paper Co. (Chengdu, China). The degree of polymerization of cellulose was 650, as measured with an Ubbelohde viscometer in cupriethylenediamine hydroxide solution. Tetrabutyl titanate [$Ti(OBu)_4$; >99.0%], *N*-methylimdazole, chloroprene (99.0%), *N,N*-methylene double acrylamide (MBA), and ammonium persulfate [$(NH_4)_2S_2O_8$; 99.0%], and 4-vinyl pyridine (4VP; >96.0%) were purchased from Aladdin Reagents Co., Ltd. (Shanghai, China). *N,N*-Dimethylformamide and 4VP were purified by vacuum distillation, and other reagents were used as received. 1-Allyl-3-methylimidazolium chloride was synthesized according to the procedure in the cited publication.[16] MMT–Na was provided by Weifang Huawei Bentonite Group Co., Ltd., without further purification. Milli-Q water, with a resistivity of 18 MΩ cm, was used in all of the experiments.

Synthesis of Cellulose-*g*-Poly(4-vinyl pyridine) (Cellulose-*g*-p4VP)/TiO_2/MMT

MMT (0.20 g) was dispersed in 10 mL of *N,N*-dimethylformamide. The dispersion was stirred for few hours and then 4VP (2.0 g) was added to the dispersion; this was termed solution 1. Solution 2 was made by the dissolution of cellulose (0.20 g) in 1-allyl-3-methylimidazolium chloride (10.0 g) at 75°C. Solution 1 was added to solution 2 dropwise, and then MBA and $(NH_4)_2S_2O_8$ were added to the mixed solution. The molar ratios of MBA/4VP and $(NH_4)_2S_2O_8$/4VP were both 0.05. The mixed solution was kept at 70°C for 4 h.

The TiO_2 sol solution was prepared by the dissolution of $Ti(OBu)_4$ (4 mL) in anhydrous ethanol (20 mL). The TiO_2 sol solution was added to the previous resultant, and then, a cellulose-*g*-p4VP/TiO_2/MMT nanocomposition was formed. The cellulose-*g*-p4VP/MMT/TiO_2 composition was filtered and dried at 70°C.

The same procedure was used to synthesize cellulose-*g*-p4VP/MMT without the addition of the TiO_2 sol solution and cellulose-*g*-p4VP/TiO_2 without the addition of MMT. Cellulose/TiO_2 was prepared by the addition of the TiO_2 sol solution to solution 2. Cellulose-*g*-p4VP was synthesized without the addition of the TiO_2 sol solution and MMT. The cellulose-*g*-p4VP was washed by methanol with a Soxhlet apparatus for 24 h and then filtered and dried at 70°C before characterization.

Characterization

Fourier transform infrared (FTIR) spectroscopy was carried out on an IR prestige-21. The samples were dried in a vacuum oven at 70°C for 24 h and then prepared by a KBr disk method. X-ray diffraction (XRD) was carried out on an X-ray diffractometer (D8 Focus, Bruker, Germany). The patterns with Cu Kα radiation ($\lambda = 1.5418$ Å) were recorded in the region of 2θ from 10 to 80° with a step speed of 6°/min. Scanning electron microscopy (SEM) images were captured on LEO-1430VP with an accelerating voltage of 20 kV. Transmission electron microscopy (TEM) images were captured on JEM-2000 (Japan) with an accelerating voltage of 100 kV. The calcination of the samples for SEM characterizations was performed at 550°C for 2 h in a muffle.

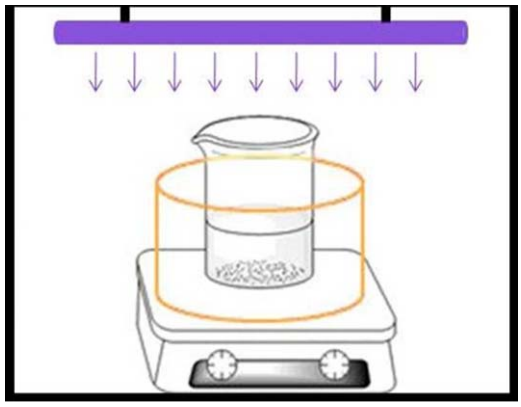

Scheme 1. Illustration of the reactor and irradiation. [Color figure can be viewed in the online issue, which is available at wileyonlinelibrary.com.]

Photocatalytic Degradation of Methyl Orange (MO)

The photocatalytic activities of cellulose-*g*-p4VP/TiO_2/MMT were evaluated by the monitoring of the degradation of MO. Cellulose-*g*-p4VP/MMT/TiO_2 powder (0.20 g) was added to 200 mL of MO solution (200 mg/L). The apparatus used in the experiments is illustrated in Scheme 1. The solution was stirred for 12 h in a dark room to ensure that the adsorption of MO had reached equilibrium. The solution was subsequently irradiated by UV light (30 W, anaerobic UV germicidal lamp, Cangzhou) at a wavelength of 254 nm. The temperature was 25°C, and the pH of the solutions was 6.5. The MO concentration was measured by the absorbance at 466 nm at a given irradiation time interval. The degradation rates (r_ds) of MO were obtained as follows:

$$r_d = A_t/A_I = c_t/c_I$$

where A_I is the initial absorbance of MO, c_I is the initial concentration of MO, and A_t and c_t are the absorbance and concentration of MO at a certain time (t). All of the experiments of the photocatalytic degradation of MO were run in triplicate to ensure reproducibility and accuracy.

RESULTS AND DISCUSSION

FTIR Spectra

The FTIR spectra of cellulose, MMT, cellulose-*g*-p4VP, cellulose-*g*-p4VP/MMT, and cellulose-*g*-p4VP/MMT/TiO_2 are presented in Figure 1. The spectrum of neat cellulose exhibited a strong and broad absorption at 3414 cm^{-1} due to the stretching vibrations of hydrogen-bonded hydroxyl groups. The characteristic absorption peaks for MMT occurred at 518 cm^{-1} (Si—O) and 463 cm^{-1} (Mg—O).[17] The FTIR spectra of cellulose-*g*-p4VP and cellulose-*g*-p4VP/MMT shown in Figure 1 showed ligand peaks at 3025 cm^{-1} (C—H stretching vibrations in the pyridine ring), 1599 and 1417 cm^{-1} (in plane C—H, and C—H wagging vibrations in the pyridine ring), and 821 cm^{-1} (symmetric ring breathing).[18] This may have indicated the successful grafting of 4VP onto cellulose. These characteristic peaks were also

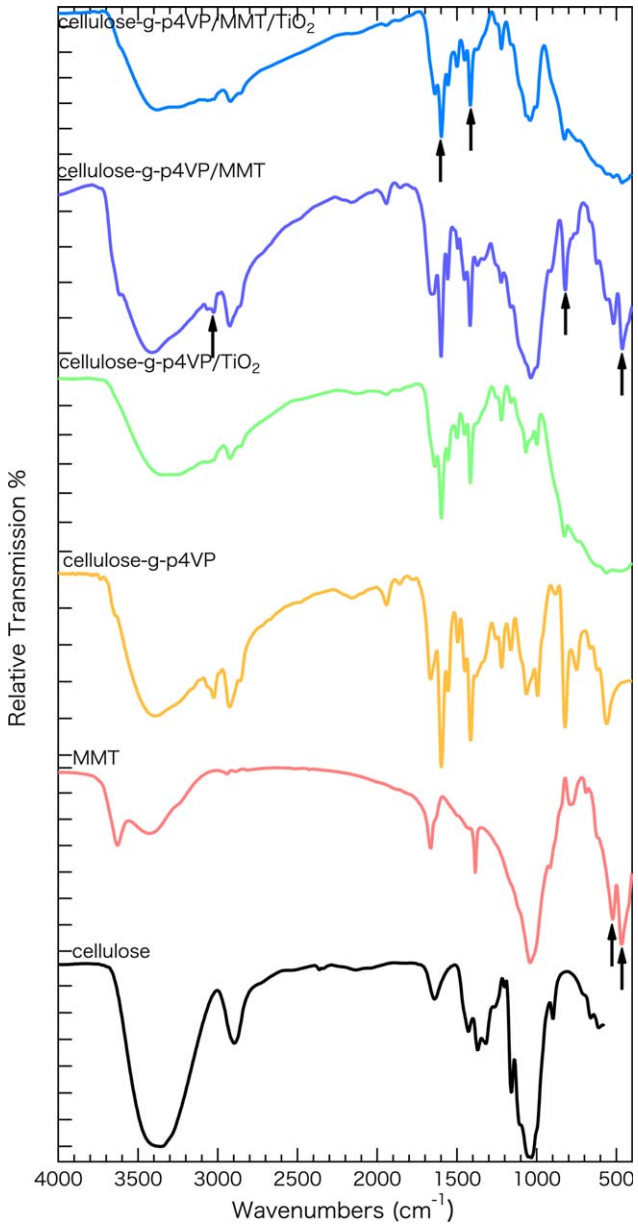

Figure 1. FTIR spectra of the neat cellulose, MMT, cellulose-*g*-p4VP/TiO_2, cellulose-*g*-p4VP/MMT, and cellulose-*g*-p4VP/TiO_2/MMT. [Color figure can be viewed in the online issue, which is available at wileyonlinelibrary.com.]

observed for cellulose-*g*-p4VP/TiO_2. Ion exchanges can be carried out between TiO_2 and MMT after the addition of TiO_2. This may have rendered the disappearance of the characteristic peaks of MMT at 518 cm^{-1} (Si—O) and 463 cm^{-1} (Mg—O).[19] However, because of the strong absorbance of TiO_2 in the range 400–700 cm^{-1}, we were not able to observe this in the corresponding spectrum. The destruction of the Si—O and Mg—O bonds indicated that the immobilization of TiO_2 on MMT was a chemical process rather than a physical doping. In the spectrum of cellulose-*g*-p4VP/MMT/TiO_2, the aforementioned characteristic peaks of pyridine were also visible; this provided a proof of the formation of the cellulose-*g*-p4VP/MMT/TiO_2 nanocomposition.

XRD Patterns

The XRD patterns of the pure TiO_2, cellulose/TiO_2, cellulose-*g*-p4VP/TiO_2, and cellulose-*g*-p4VP/MMT/TiO_2 are presented in Figure 2. The anatase TiO_2 had a characteristic diffraction peak at 25.16°; this corresponded to the (101) crystal plane, which was observed both for anatase TiO_2 and cellulose-*g*-p4VP/MMT/TiO_2, as presented in Figure 2. For the pure TiO_2, the diffraction peaks of other crystal planes were assigned in Figure 2; these were consistent with the XRD pattern of anatase TiO_2.[20] These crystal peaks were also observed for cellulose/TiO_2. For cellulose-*g*-p4VP/TiO_2 and cellulose-*g*-p4VP/MMT/TiO_2, the other peaks of anatase TiO_2 were not detectable because of the low intensity. This result also confirmed that anatase TiO_2 could be synthesized at low temperature without calcination.

TEM and SEM Characterization

We also compared the morphologies of cellulose/TiO_2 and cellulose-*g*-p4VP/TiO_2 before and after calcination. Figure 3(a,b) corresponds to the morphology of the cellulose/TiO_2 samples before and after calcination, respectively. The precursor of TiO_2 could bind to the cellulose and form nanoparticles in the coil configuration. This is clearly shown in Figure 3(a,b). The cellulose/TiO_2 composite was about a few micrometers with porous features, as presented in Figure 3(a). Through calcination, cellulose was decomposed, and only TiO_2 remained in the sample. The SEM image in Figure 3(b) shows the TiO_2 clusters formed on the cellulose template. The TiO_2 particles were much smaller compared to the cellulose template, where the particles were embedded.

The SEM images of cellulose-*g*-p4VP/TiO_2 before and after calcination are presented in Figure 3(c,d), respectively. The morphology of cellulose-*g*-p4VP/TiO_2 was rather different compared to the morphology of cellulose/TiO_2 presented in Figure 3(a). The cellulose-*g*-p4VP/TiO_2 composite exhibited a solid feature with a flake shape as shards on the scale of few micrometers. The particles were fragmented after calcination, despite the fact that the morphologies of the cellulose-*g*-p4VP/TiO_2 composites were almost identical. This indicated that the chemical

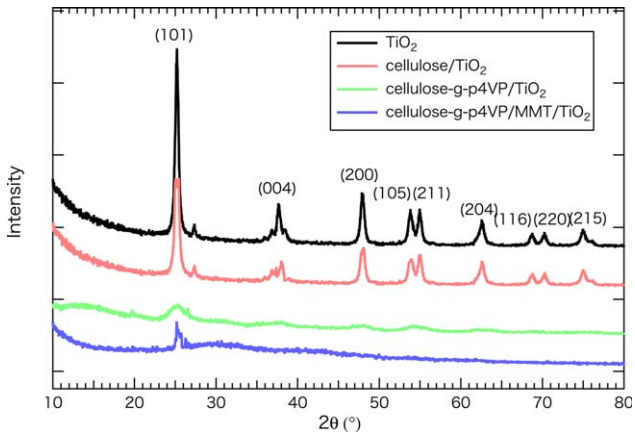

Figure 2. XRD patterns of the pure anatase TiO_2, cellulose/TiO_2, cellulose-*g*−4VP/TiO_2, and cellulose-*g*-p4VP/MMT/TiO_2. [Color figure can be viewed in the online issue, which is available at wileyonlinelibrary.com.]

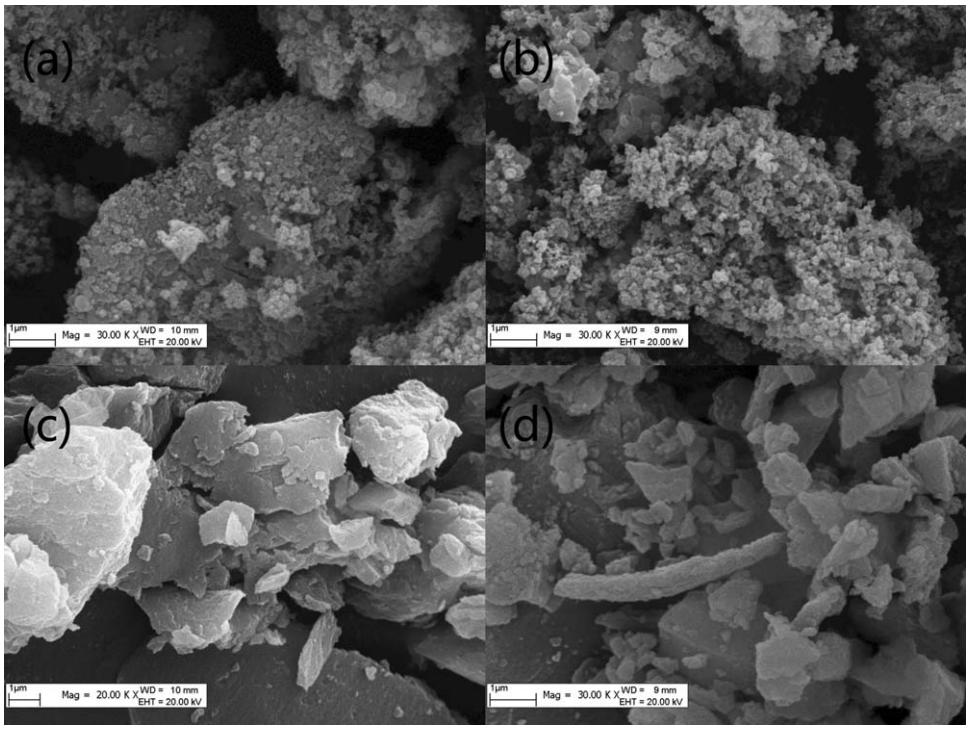

Figure 3. SEM images of cellulose/TiO_2 and cellulose-*g*-p4VP/TiO_2: (a,b) cellulose/TiO_2 composite before and after calcination and (c,d) cellulose-*g*-p4VP/TiO_2 composite before and after calcination. The scales in the images represent 1 μm.

modification of the celluloses had strong impact on the morphology of the TiO_2 compositions. Positive charges were introduced by the grafting of 4VP on cellulose, and the increase in the charge density rendered the change in the chain configuration and, consequently, the morphology of the nanocomposite.

Figure 4(a,b) presents the SEM and TEM images of the cellulose-*g*-p4VP/MMT/TiO_2 composite. The SEM image shows that the morphology of the cellulose-*g*-p4VP/MMT/TiO_2 composite was mainly flakes and was similar to the shape presented in Figure 3(c) with better dispersion. This may have indicated that the morphology of cellulose-*g*-p4VP/MMT/TiO_2 was primarily caused by the addition of the grafted cellulose. The addition of MMT, however, had very little effect. The TEM image shown in Figure 4(b) exhibited the morphology of the cellulose–MMT intercalation. The well-intercalated composite exhibited a thin-layer structure and was composed of flakes, as presented in Figure 4(a). This thin-layer structure benefited the synthesis of TiO_2, and the TiO_2 particles could be evenly immobilized on the structure; as a result, the adsorption increased, and this led to an efficient photocatalytic degradation of organic pollutants.

Photocatalytic Degradation of MO

Organic pollutants can be eliminated from water and air with TiO_2 particles as a photocatalyst under UV radiation. The TiO_2 particles engage in photocatalytic reaction because of the high oxidation capacity of the photogenerated holes. In this study, the photocatalytic degradation of MO was demonstrated as an application of the cellulose-*g*-p4VP/MMT/TiO_2 nanocomposite. The degradation of MO involves two processes: adsorption and photocatalytic degradation. These two processes were studied separately, and the photocatalytic degradation capacities with cellulose/TiO_2, cellulose-*g*-p4VP/TiO_2, and cellulose-*g*-p4VP/MMT/TiO_2 were also compared.

The results of the photocatalytic degradation of MO are presented in Figure 5 as a function of the time. First, the photocatalytic degradation without the addition of the nanocomposites was studied. It is shown in Figure 5 that MO could not be self-degraded under UV radiation within 100 h. In the presence of the cellulose-*g*-p4VP/MMT/TiO_2 nanocomposite without UV radiation, an abrupt decrease in the MO concentration was observed in 12 h, and the curve leveled off afterward. This indicated that the adsorption of MO was able to reach equilibrium in 12 h. The experiment was performed for cellulose-*g*-p4VP/MMT with UV radiation, whereas only the adsorption process was observed. The same experiment was carried out with cellulose-*g*-p4VP/MMT/TiO_2, and complete degradation was observed. The results suggest that the two processes, adsorption and degradation, acted synergistically.

In the previous section, we showed that the morphology of the nanocomposite changed with the addition of the grafted cellulose. The differences in photocatalytic degradation in the presence of cellulose/TiO_2, cellulose-*g*-p4VP/TiO_2, and cellulose-*g*-p4VP/MMT/TiO_2 were also compared, and the results are presented in Figure 6. The curves in Figure 6 clearly demonstrate two groups of results, one with a low degradation percentage and the other with nearly complete degradation. The degraded MO was only about 30% for the cellulose/TiO_2 nanocomposite, and as shown in Figure 6, the MO concentration changed linearly with time. In the other group, nearly complete degradation

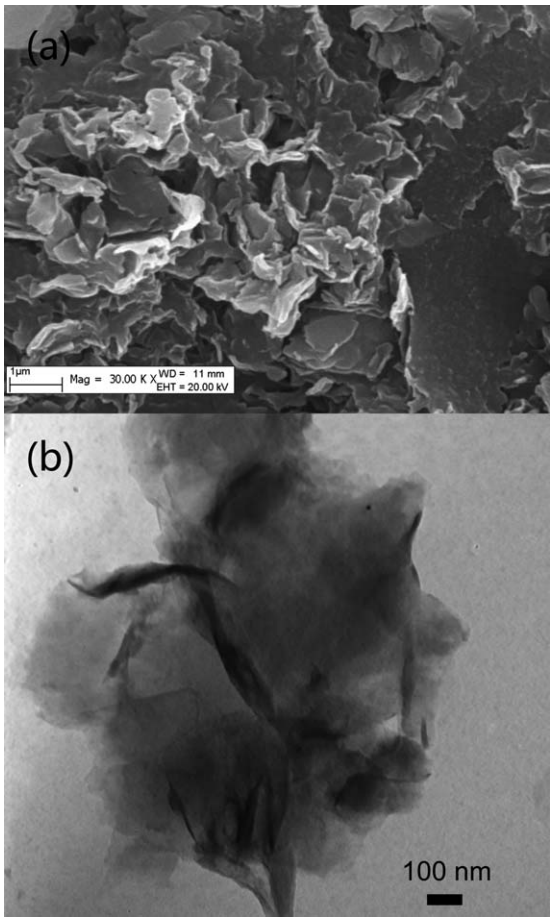

Figure 4. (a) SEM image and (b) TEM image of the cellulose-*g*-p4VP/MMT/TiO_2 nanocomposite.

of MO was reached with the presence of cellulose-*g*-p4VP/TiO_2 and cellulose-*g*-p4VP/MMT/TiO_2. For cellulose-*g*-p4VP/TiO_2, the degraded MO was about 90%, and for cellulose-*g*-p4VP/MMT/TiO_2 the value was 98%. In the group, an abrupt decrease in the MO concentration occurred before the initial 12 h because of the adsorption process (Figure 5), and then, it was followed by a slow decrease because of photocatalytic degradation. In the later process, the cellulose-*g*-p4VP/TiO_2/MMT nanocomposite appeared to be more effective compared to the cellulose-*g*-p4VP/TiO_2 nanocomposite.

These results suggest that the effect of the addition of the grafted cellulose was significant. It can be understood as follows. The reaction of the photocatalytic degradation occurred locally on the surface of the TiO_2. This required the accumulation of organic pollutants on the surface. In view of the fact that there was no special interaction between TiO_2 and the organic pollutants, the photocatalytic reaction relied on the random collision of the TiO_2 particles and the organic molecules. This may have caused a low efficiency of the photocatalytic degradation of MO in the bulk. The neat cellulose did not present the feature of adsorbing MO, and then, it resulted in a slow degradation of MO. Through the introduction of 4VP onto the cellulose backbone, MO could bind to pyridine by complexation. It significantly increased the reaction rate of the photocatalytic degradation.

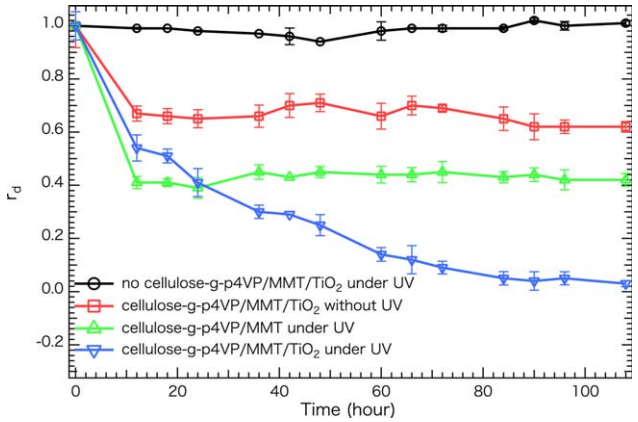

Figure 5. Degradation of MO as a function of the time under different initial conditions. The quantities of cellulose-*g*-p4VP/MMT, cellulose-*g*-p4VP/MMT/TiO_2, and MO used in the experiment were 0.2, 0.2, and 0.04 g, respectively. [Color figure can be viewed in the online issue, which is available at wileyonlinelibrary.com.]

The kinetics of the photocatalytic degradation were studied with different initial concentrations of MO. As mentioned previously, two processes were involved: adsorption and photocatalytic degradation. To study the kinetics of the photocatalytic degradation of MO, we assumed that when the adsorption reached equilibrium, the photocatalytic reaction was the rate-determining step. The equilibrium of the adsorption was reached before 12 h; thus, the changes in the MO concentration were able to reveal the reaction rate of photocatalytic degradation. The logarithms of the concentration changes are presented as a function of the time in Figure 7 with three initial concentrations of MO, and a linear dependence was observed. This indicated that the photocatalytic degradation of MO followed pseudo-first-order kinetics. Thus, the data were interpreted with the integrated form of the pseudo-first-order rate equation:

$$\ln\frac{c_I}{c_t} = k * t + a$$

where k is the apparent rate constant and a is a parameter due to the initial adsorption of MO. The values of the parameters

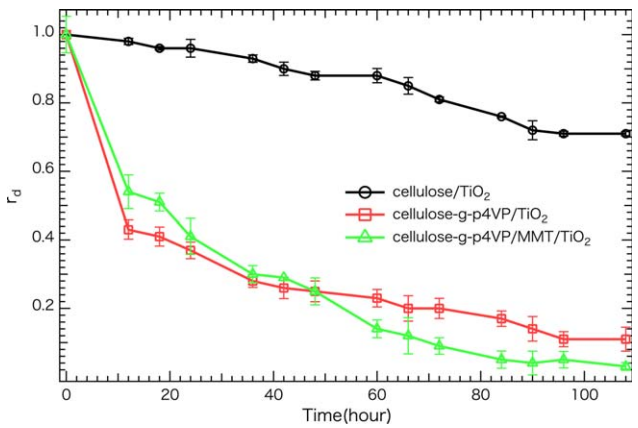

Figure 6. Degradation of MO by cellulose/TiO_2, cellulose-*g*-p4VP/TiO_2, and cellulose-*g*-p4VP/MMT/TiO_2 as a function of the time. [Color figure can be viewed in the online issue, which is available at wileyonlinelibrary.com.]

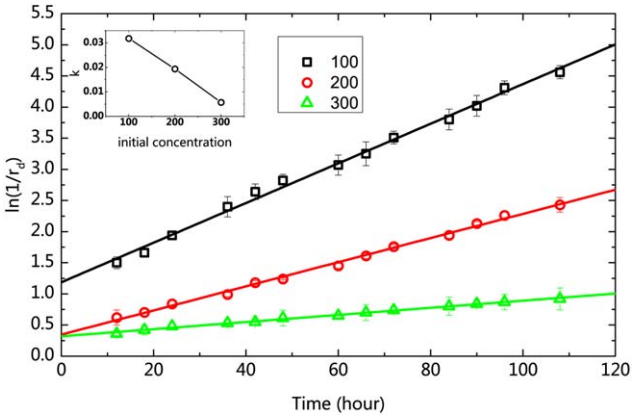

Figure 7. Pseudo-first-order photocatalytic degradation of MO on the cellulose-*g*-p4VP/MMT/TiO_2 nanocomposite as a function of the initial MO concentration: 100, 200, and 300 mg/L. The apparent degradation rate is plotted as a function of the initial concentration of MO in the inset. [Color figure can be viewed in the online issue, which is available at wileyonlinelibrary.com.]

obtained from linear regression are presented in Table I. The parameter c_{IA} is the concentration of MO at $t = 0$, and the decrease in the concentration of MO was due to adsorption. As presented in Table I, c_{IA} at the equilibrium of adsorption increased with the initial concentration of MO. The results suggest that the increase of the initial concentration of MO led to slow photocatalytic degradation, as shown in the panel of Figure 7.

CONCLUSIONS

The cellulose-*g*-p4VP/TiO_2/MMT nanocomposite photocatalyst was fabricated successfully by intercalation polymerization and a sol–gel method at low temperature. Anatase TiO_2 could be firmly immobilized on MMT through an ion-exchange reaction. The nanocomposite with the grafted cellulose as a template exhibited a very different morphology compared to that using neat cellulose. The nanocomposite demonstrated photocatalytic activity in the degradation of MO. The photocatalytic activity followed the order: Cellulose-*g*-p4VP/MMT/TiO_2 > Cellulose-*g*-p4VP/TiO_2 > Cellulose/TiO_2. The introduction of MMT not only improved the adsorbing–degrading performance of cellulose-*g*-p4VP/MMT/TiO_2 but also made the photocatalyst easy to separate. The kinetic studies suggest that the reaction followed pseudo-first-order photocatalytic degradation. The reaction rate decreased with the initial concentration of MO. The photodegradation rate can be faster at a lower concentration of MO. This study may be an example of the synthesis of different morphologies of TiO_2 or other metal oxides with grafted cellulose as a template; this may improve the photocatalytic ability in dealing with organic pollutants.

Table I. Pseudo-First-Order Rates Obtained by the Linear Regression Shown in Figure 7

c_I (mg/L)	k (h^{-1})	a	c_{IA} (mg/L)[a]
100	0.03183	1.18603	30.54314
200	0.01938	0.34627	141.4643
300	0.00572	0.31894	218.07575

[a] The value was calculated as follows: $c_{IA} = c_I \times e^{-a}$.

ACKNOWLEDGMENTS

One of the authors (W.W.) thanks the Qianren Project for financial support. Another author (R.W.) thanks the National Natural Science Foundation of China (contract grant number 51063007) for its financial support.

REFERENCES

1. Kumar, S. G.; Devi, L. G. *J. Phys. Chem. A* **2011**, *115*, 13211.
2. Hashimoto, K.; Irie, H.; Fujishima, A. *Jpn. J. Appl. Phys. Part 1* **2005**, *44*, 8269.
3. Venkataramanan, N. S.; Matsui, K.; Kawanami, H.; Ikushima, Y. *Green Chem.* **2007**, *9*, 18.
4. Lu, Y.; Sun, Q. F.; Liu, T. C.; Yang, D. J.; Liu, Y. X.; Li, J. *J. Alloys Compd.* **2013**, *577*, 569.
5. Natarajan, T. S.; Natarajan, K.; Bajaj, H. C.; Tayade, R. J. *J. Nanopart. Res.* **2013**, *15*, 1669.
6. Xiang, Q. J.; Yu, J. G.; Jaroniec, M. *Chem. Commun.* **2011**, *47*, 4532.
7. Liu, S. L.; Tao, D. D.; Zhang, L. N. *Powder Technol.* **2012**, *217*, 502.
8. Yu, D. H.; Yu, X. D.; Wang, C. H.; Liu, X. C.; Xing, Y. *ACS Appl. Mater. Interfaces* **2012**, *4*, 2781.
9. Valera-Zaragoza, M.; Yescas-Yescas, A.; Juarez-Arellano, E. A.; Aguirre-Cruz, A.; Aparicio-Saguilan, A.; Ramirez-Vargas, E.; Sepulveda-Guzman, S.; Sanchez-Valdes, S. *Polym. Bull.* **2014**, *71*, 1295.
10. Cui, Y. M.; Liu, L.; Li, B.; Zhou, X. F.; Xu, N. P. *J. Phys. Chem. C* **2010**, *114*, 2434.
11. Crippa, M.; Callone, E.; D'Arienzo, M.; Muller, K.; Polizzi, S.; Wahba, L.; Morazzoni, F.; Scotti, R. *Appl. Catal. B* **2011**, *104*, 282.
12. Wang, Q. Q.; Wang, X.; Li, X. J.; Cai, Y. B.; Wei, Q. F. *Appl. Surf. Sci.* **2011**, *258*, 98.
13. Tahir, M.; Amin, N. S. *Chem. Eng. J.* **2013**, *230*, 314.
14. Liao, C. N.; Wu, Q.; Su, T.; Zhang, D.; Wu, Q. S.; Wang, Q. G. *ACS Appl. Mater. Interfaces* **2014**, *6*, 1356.
15. Kasgoz, H.; Ozbas, Z.; Esen, E.; Sahin, C. P.; Gurdag, G. *J. Appl. Polym. Sci.* **2013**, *130*, 4440.
16. Zhang, H.; Wu, J.; Zhang, J.; He, J. *Macromolecules* **2005**, *38*, 8272.
17. Tahir, M.; Amin, N. S. *Appl. Catal. B* **2013**, *142*, 512.
18. Urena, F. P.; Gomez, M. F.; Gonzalez, J. J. L.; Torres, E. M. *Spectrochim. Acta A* **2003**, *59*, 2815.
19. Mallakpour, S.; Asadi, P. *Polym. Bull.* **2012**, *68*, 53.
20. Reyes-Coronado, D.; Rodriguez-Gattorno, G.; Espinosa-Pesqueira, M. E.; Cab, C.; de Coss, R.; Oskam, G. *Nanotechnology* **2008**, *19*, 145605.